Overcoming Conductivity-Stretchability Tradeoff in Soft Conductive Composites Through Liquid Metal Junctions

Aminur Rahman, Mohammad Madadi, Jiexian Ma, Pu Zhang*

Department of Mechanical Engineering, State University of New York at Binghamton, Binghamton, NY 13902, United States

ABSTRACT: Soft conductive composites are significant components of soft and wearable electronics. Existing soft conductive composites encounter difficulties in attaining 10% of copper's electrical conductivity whilst maintaining high stretchability meanwhile. In this work, a novel 'soft conductive junction' concept is introduced to overcome the conductivity-stretchability tradeoff. This new paradigm of soft conductive composites consists of an interwoven copper fiber network embedded in a compliant elastomer matrix. The fiber junctions are connected using liquid metal bridge, which significantly lowers the junction resistance without influencing the stretchability of the fiber network. These hybrid composites uphold ultra-high and strain-insensitive conductivity that is around 60,000 S/cm under 55-75% stretch. Notably, the conductivity and stretchability of such composites can be tailored through prestrain. Potential applications of the composites in stretchable circuitry, wearable interconnects, capacitance tactile sensors, and highly stretchable Joule heaters are presented.

KEYWORDS: soft conductive composite, soft junction, liquid metal, soft electronics, Joule heaters

1. INTRODUCTION

Soft conductive composites are widely used in soft electronics,[1,2] flexible and wearable electronics,[3–5] transparent electrodes,[6–10] smart sensors,[11–13] and soft robotics.[14–16] In practice, soft conductive composites[17–19] desire high electrical conductivity, stretchability or flexibility, strain-insensitivity, and cyclic stability. In recent years, several approaches have evolved to develop high-performance soft conductive composites.[12] The Ashby chart in **Figure 1d** compares the performance of several major types of soft conductive composites including hard filler,[20] liquid metal (LM),[21] and hybrid solid-liquid filler composites.[22] The hard filler composites usually consist of silver or gold nanomaterials[23,24] as primary conductive networks. Such hard filler composites exhibit excellent initial conductivity but their resistance increases significantly under stretch[20] due to damage, resulting in limited strain-insensitive stretchability. Their overall performance also deteriorates quickly under cyclic stretching or bending.[12,25] To circumvent the rigidity-mismatch issue in hard filler composites, researchers developed liquid filler composites with LMs as the most popular filler for their good conductivity (3-3.5×10^4 S/cm).[26] LM composites have improved strain-insensitive stretchability compared to hard-filler composites but still suffer from bottlenecks such as limited conductivity or strain-sensitive conductivity.[11,27,28] Overall, there is a conductivity-stretchability tradeoff for soft conductive composites containing only hard or liquid fillers.[19,29] A possible solution is to adopt a hybrid filler approach that combines the advantages of solid and liquid fillers and achieve both high conductivity and stretchability simultaneously.[30–33] This hybrid filler approach is still an emerging field with new materials being reported. Nevertheless, the existing hybrid filler composites also encounter difficulties in attaining strain-insensitive conductivity[34] targeting 4-6×10^4 S/cm (as compared to copper, 6×10^5 S/cm)

whilst maintaining at least 30% cyclic stretchability for applications in flexible and wearable electronics. This work aims at targeting this limit.

Principally, hybrid filler composites utilize the synergy of multiple percolation networks, usually a primary network (e.g., silver nanoflakes or nanowires) with high conductivity and a secondary network (e.g., LM nanodroplets) with high stretchability. The overall conductivity of the composite mainly depends on the microstructure[33] and percolation of the primary network.[35] So the primary network prefers hard metal materials with large aspect ratios, i.e., wires/fibers[36] rather than particles/flakes. [22,30,37] As to the percolation, the contact resistance between hard fillers is a limiting factor[38] for electrical conductivity. Therefore, in order to discover hybrid filler composites with high performance, we need to not only design the microstructure of the primary network but also tackle the contact resistance issue. Considering that we aim to obtain conductivity comparable to 10% of copper, a woven fiber network is an ideal microstructural design for the primary network given its high stretchability and high-volume ratio. In contrast, the well-studied lattice materials usually do not sustain much stretchability.[38,39] As regard to the inter-fiber junctions of a woven fiber network, researchers used to weld them to reduce the high contact resistance,[40–43] i.e. the hard junction approach in **Figure 1c**. An intermetallic bridge[44] approach was also utilized to reduce contact resistance but strain-insensitivity was not achieved due to the rigidity of the junction. Such a hard junction approach inevitably increases the junction rigidity and devastates the stretchability of the network.[43,45,46] To overcome this issue, we propose a LM-based soft junction concept in this work, as shown in **Figure 1c**. For the soft junction approach, the fiber junctions are connected by LM bridges (**Figure S6**, Supporting Information), which are fluidic and conductive. This new approach not only mitigates the contact resistance but also retains the mobility of the fiber junctions and the woven fiber network.

Using this 'soft conductive junction' concept, we introduce a new class of copper-LM composites (CuLMCs) with ultra-high and strain-insensitive conductivity, high stretchability, and excellent cyclic stability. The CuLMCs consist of a woven copper mesh, LM-based soft junctions, and a compliant elastomer matrix. The stretchability of CuLMC is attributed to the mesh geometry (**Figure 1a**) and the conductivity improvement is derived from the LM-based soft junctions. The Ashby chart in **Figure 1d** and **Figure S12** (Supporting Information) compares the electrical conductivity of CuLMCs and state-of-the-art composites in the literature. Most composites exhibit strain-insensitive conductivity in the range of 1,000-20,000 S/cm. The fabricated CuLMCs can provide strain-insensitive conductivity exceeding 10% of copper (up to 77,000 S/cm). Depending on the opening rate and prestrain, it is also capable to provide very high stretchability up to 180%. In some cases, CuLMCs can achieve conductivity around 60,000 S/cm under 45-70% stretch, which are remarkable records for soft conductive composites. **Figure 1b** shows the role of LM junctions on the conductivity improvement for copper mesh composite (CuC) without LM junctions, original CuLMCs, and prestrained CuLMCs. Usually, 20- to 60-fold of conductivity improvement was found by adding LM junctions. Moreover, the overall electrical conductivity and stretchability of CuLMCs can be tailored by tuning the geometric pattern, fiber thickness, opening rate, and prestrain. With such remarkable records of conductivity, stretchability, and tailorability, CuLMCs have promising applications in soft and wearable electronics, not to mention their facile and low-cost manufacturability.

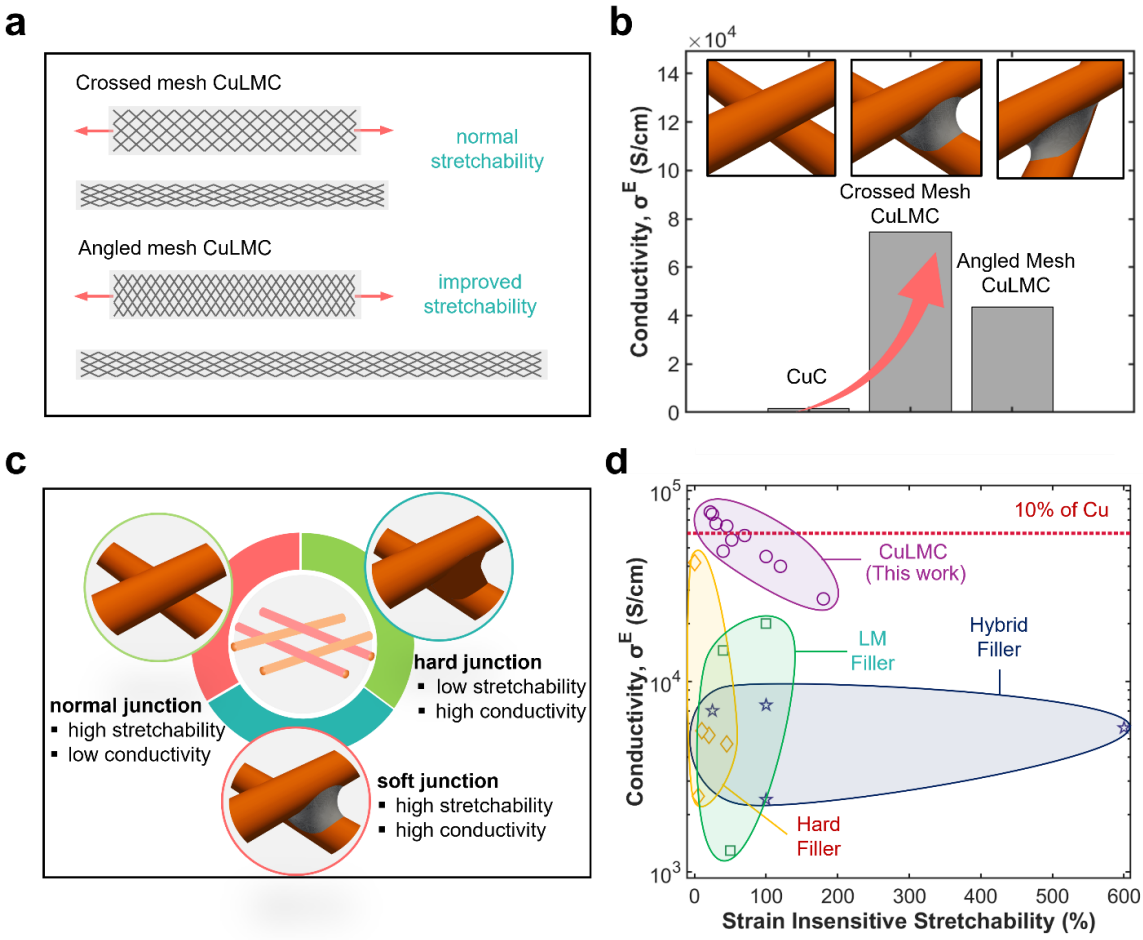

Figure 1. a) The CuLMC consists of a stretchable copper mesh embedded in an elastomer matrix. The stretchability can be enhanced dramatically by using angled mesh (detailed in **Figure S1**, Supporting Information). b) The LM junctions significantly increase electrical conductivity of the composites by reducing junction resistance. Usually, 20-60 fold of conductivity improvement is observed. c) Comparison of the electromechanical characteristics of different junction types: normal, hard, and soft junction. The normal and hard junctions suffer from stretchability-conductivity tradeoff as either low conductivity or low stretchability. The LM-based soft junction overcomes this tradeoff and attains high stretchability and conductivity simultaneously. d) This Ashby chart compares the electrical conductivity and strain-insensitive stretchability of soft conductive composites: hard filler ◊, LM filler □, hybrid filler ☆, CuLMC ○. The CuLMCs exhibit very high conductivity exceeding 10% of Cu. Detailed data are tabulated in **Table S2**, Supporting Information.

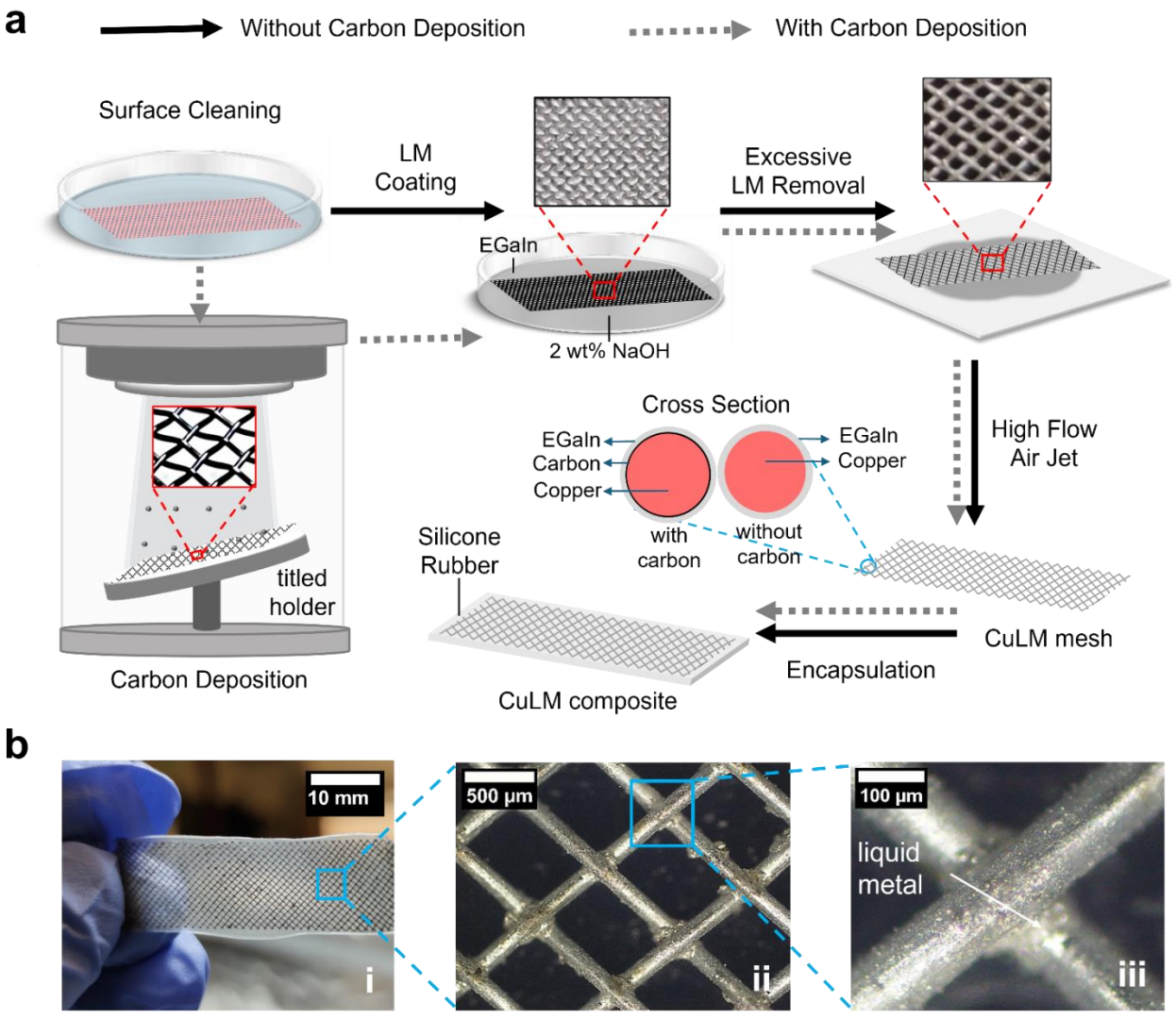

Figure 2. The fabrication process of CuLMCs. Two different approaches are employed: approach 1 without carbon deposition and approach 2 with carbon deposition. a) In approach 1, the process sequentially consists of surface cleaning, LM coating, removal of excessive LM, and PDMS encapsulation. For approach 2, approximately 10 nm of carbon is deposited by thermal evaporation process before the LM coating step. b) Optical microscopy images of fabricated CuLMCs. LM fills in the fiber junctions and forms a soft liquid bridge. There is an ultra-thin layer of LM residual on the fiber as well, which has negligible contributions to the electrical conductivity.

2. EXPERIMENTAL SECTION

2.1 Materials. In this work, four different sizes of copper mesh (#20, #30, #40, #60) were used. The mesh sample was cut into small pieces diagonally (45° along the fiber direction) from the bulk woven mesh (Laohu and Skypro, China). The fiber diameters and opening rates are shown in **Table S1**, Supporting Information. NaOH was acquired from Fisher Scientific. Eutectic gallium-indium (EGaIn, $Ga_{75.5}In_{24.5}$) was obtained by alloying Ga and In metals (RotoMetals Inc.) in an oven. The silicone rubber Ecoflex 00-30 was from Smooth-On.

2.2 Composites without Carbon Coating. To fabricate CuLMCs, copper mesh was sectioned diagonally at a 45° angle relative to the fiber orientation from a larger stock. The surface was rinsed with deionized water for 2 min to remove unwanted impurities from the mesh surface. Afterward, the mesh was dried on a hotplate at 40°C for 2 min. The LM coating bath consists of 2wt.% aqueous NaOH and EGaIn. Initially, the surface tension of LM would prevent it from spreading over the mesh surface and junctions spontaneously. Gentle rubbing was applied until LM spreads all over the surface. Nevertheless, the pores of copper mesh were also filled with LM as depicted in **Figure 2a** (top middle). The excessive LM was then meticulously removed by wiping with filter paper. High-pressure air jet was also applied to ensure proper removal. After removing excessive LM, the mesh pores are clear and LM predominately accumulates near junctions, as shown in **Figure 2b** (bottom right) and **Figure S6**, Supporting Information. To manufacture prestrained CuLMCs, the angled mesh (**Figure S1**, Supporting Information) is used. For encapsulation, the LM-coated copper mesh is fixed on a glass slide and Ecoflex 00-30 is spread on the surface followed by vacuum degassing for 5 min (VWR vacuum oven) to remove air bubbles. The assembly was subsequently sandwiched with another glass slide and clamped. The system was cured at 65°C for

4 hours on a hot plate, followed by room temperature curing for 12 hours to obtain the final composite samples. A similar procedure was followed to fabricate brass-LM composites for the Joule heating applications. No carbon coating is applied to the brass mesh.

2.3. Composites with Carbon Coating. In addition, for composites with anti-aging behavior, the copper mesh was deposited with a thin layer of carbon before LM coating. This additional layer of carbon serves as a barrier between Cu and LM, enhancing the durability and functional lifespan of the CuLMCs. Specifically, the cleaned and dried copper mesh is coated with carbon coating (108carbon Cressington Scientific Instruments) under 10^{-4} mbar vacuum pressure. To produce plasma, a 100mA current was supplied for 5 seconds. Approximately 10nm carbon coating was deposited on each side of the copper mesh. In the deposition process, a tilted sample holder was used for better carbon particle distribution on the 3D structure.

2.4. Tensile Testing. Rectangular specimens (60mm × 11mm) were tested on a tensile tester (eXpert 4000, ADMET Inc.) with a 5N load cell. Initial gauge length of 40mm and an extension rate of 0.5mm/sec were used. For each sample, at least three specimens were tested.

2.5. IR Imaging. Thermal images were taken using a pair of FLIR camera (E5 and A310) and processed by FLIR tools software and MATLAB.

2.6. Electromechanical Testing. The electromechanical behavior of the composites was characterized by performing mechanical and electrical testing simultaneously in a synchronized way. A four-wire setup (see **Figure S9a**, Supporting Information) was built to measure the electrical resistance using a Keithley 2110 digital multimeter and Aglient E3612A DC power supply. Two ends of the CuLMC sample were connected to additional wiring using copper tape, and insulated by double-sided tape and adhesive tape. The thickness of each CuLMC specimen was measured using an optical microscope. The electrical conductivity was calculated from the

formula $\sigma^E = L/(RWt)$, where L, W, t, R are respectively length, width, thickness, and resistance of the composite specimen.

The bending test was conducted by a setup (**Figure S9b** and **S9c**, Supporting Information) using 3D printed substrates with designed radii for each type of samples. The required radius was calculated from the formula, $\varepsilon_b = \left(t_{support} + t_{sample}\right)/2r$, where $t_{support}$, t_{sample}, r are respectively thickness of support, sample thickness, and substrate radius. Resistance was measured by a Keithley 2110 digital multimeter. For cyclic testing, a triangular strain profile was used with a 0.5mm/sec extension rate and 15% strain amplitude.

2.7. Fabrication of Interconnects, Capacitive Pressure Sensor, Flexible Heaters and Heat Activated Actuators. LM-coated copper mesh was cut into required shapes (rectangular strip) and connected to the LED using conductive copper paste (843WB, MG Chemicals). The stretchable circuit was obtained by encapsulating the assembly into Ecoflex 00-30.

The capacitive pressure sensor was designed as a sandwich structure, using polyurethane foam (500μm thick) embedded between two CuLMC layers on top and bottom. A slicer (SliceMaster, Jasco Inc.) was used to slice the polyurethane foam at the required thickness. All the layers were bonded together with adhesive. The rectangular sensor (10mm × 10mm) was tested for various compression modes, such as tapping, pressure variance, and object grabbing. The data was recorded as a function of capacitance using the Keithley 2110 digital multimeter.

The #30 mesh brass-LM (conductivity is 14166 S/cm, which is approximately 10% of pure Brass) composite strip was precisely tailored into narrow dimensions (80mm × 8mm) to enable conformal attachment onto curved surfaces, including human knee and cylindrical substrates. For the transparency heat actuator, a brass-LM composite formed the structural core, encapsulated within a PDMS/Paraffin Wax (PW) matrix. To achieve thermally induced bending actuation, the

entire assembly was mechanically stretched, and a thin PW layer was uniformly deposited onto the composite. Upon solidification of the PW, the actuator was further encapsulated within an additional PDMS layer to ensure structural integrity and responsive performance.

3. **RESULTS AND DISCUSSIONS**

3.1. Microstructures. The fabrication process of CuLMCs is illustrated in **Figure 2a** and introduced in the Materials and Methods section. As shown in **Figure 2b**, LM in CuLMCs predominantly gathers near the fiber junctions, serving as a conductive liquid bridge to reduce the contact resistance. In **Figure 2b**, LM clearly forms a meniscus in the junctions and shows excellent wetting condition with the copper fibers. Such a good wetting condition is partially attributed to the $CuGa_2$ intermetallic formed at the interfaces. If other metal mesh is employed, the wetting condition will vary, and LM junctions may not form properly. Our preliminary results indicate that stainless steel mesh does not wet well with LM. From **Figure 2b**, there is an ultrathin layer of LM surrounding the fibers as residuals from the LM coating process. This residual layer has negligible influence on the electrical conductivity of the composite. The CuLMC is highly stretchable because of the unique geometric feature of the woven mesh. Under uniaxial stretch, the fibers can rotate freely to accommodate the longitudinal strain. The advantage of this soft junction concept is that LM in the junction allows the fibers to rotate freely, as opposed to a hard junction that constrains the fiber rotation. When the deformation is released, the junction recovers to its original shape with the LM bridge flowing back meanwhile. The morphology of the LM bridge is discussed in **Figure S6e**, Supporting Information. Note that the soft silicone matrix plays an indispensable role on the functionality as it helps to confine LM in the junction without compromising electrical conductance (**Figure S6d**, Supporting Information), which shows stable electromechanical performance under cyclic loadings. In the fabrication process, the copper mesh is sandwiched between two glass slides. Therefore, the thickness of the composite film is twice of the fiber diameter. For composites with different mesh sizes, we have recorded a thickness of 160μm,

200μm, 220μm, and 300μm, respectively, for mesh #60, #40, #30, and #20 CuLMCs. In practice, thicker samples can be prepared by laminating multiple layers of metal mesh together.

3.2. Mechanical and Electromechanical Behaviors. The mechanical behaviors of the CuLMCs are characterized and compared to that of the copper mesh composites (CuCs), i.e., the ones without LM junctions. Experimental data (**Figures S7a** and **S7c**, Supporting Information) show that the stress-strain behavior of the composites with (CuLMCs) and without (CuCs) LM junctions are nearly identical, implying that the LM junctions do not have noticeable impact on mechanical performance. Overall, the composites behave like a hyperelastic material, similar to the Ecoflex 00-30 matrix. Mechanically, the composites undergo three different stages under uniaxial loading, as fiber rotation, fiber interlocking, and fiber pullout failure (**Figure S7a** and **S7c**, Supporting Information). Regarding the stress-strain curves, the interlocking stage starts with rapid increase of stress and ends at the peak stress where fiber pullout occurs. From the application perspective, the composites should usually be operated in the fiber rotation stage to mitigate damage.

The stretchability of CuLMCs mainly depends on their mesh sizes, or more precisely, the opening rate. Each mesh size has a different opening rate (**Table S1**, Supporting Information), a parameter indicating how dense the fibers are (**Figure 3f**, top row). For a higher opening rate, the fibers can rotate more freely before interlocking, which leads to higher stretchability of the composite. This relation is illustrated in **Figure 3b**, where the mesh #20 one has the highest opening rate and thus the stretchability. The stretchability relation in **Figure 3b** is also confirmed by the stress-strain curves in **Figure 3d** for CuLMCs with different mesh sizes. Typical microstructures before and after stretching are compared in **Figure 3f** as well.

The LM junctions completely change the electrical properties of the CuLMCs. The high junction resistance of copper mesh leads to poor electrical conductivity, but the LM junctions effectively mitigate the junction resistance (**Table S5**, Supporting Information) and boost the conductivity. As depicted in **Figure 3a** (and **Figure S5b**, Supporting Information), our data show that the LM junctions increase the conductivity by 20- to 60-fold. More specifically, the highest and lowest conductivity is observed for mesh #60 composite (77,000S/cm) and mesh #20 composite (45,000S/cm), respectively. By comparing to the conductivity of pure copper (596,000S/cm),[47] CuLMCs can readily surpass 10% of Cu's conductivity, a value hard to reach for soft conductors. The electrical conductivity is also correlated to the opening rate of the mesh (see **Figure 3c**) as a higher opening rate leads to lower conductivity. Note that the conductivity is mostly dominated by the LM junctions, not the residual LM coating covered on the mesh (**Figure S6c**, Supporting Information)

Besides the high conductivity and stretchability, another prominent feature of CuLMCs is their strain-insensitive conductivity (or resistance). The conductivity-strain relations are tested and depicted in **Figure 3e**. In the fiber rotation stage (**Figure S1a-b** and **Figure S6a**, Supporting Information) the electrical conductivity is almost constant under stretch (also in **Figure S6c**, Supporting Information), which is very useful for soft electronics applications. A sudden decline of conductivity usually occurs in the fiber pullout failure stage (close to peak stress), because of the microstructural damage in the composite. The strain-insensitive conductivity is mainly due to the unique geometric characteristic of the CuLMCs. Firstly, although the mesh geometry is distorted under stretch, the percolation network (**Figure S6a** and **Figure S6c**, Supporting Information) remains the same so the resistance does not change. Secondly, the LM junction has mitigated the contact resistance (**Figure S6b** and **Figure S6e**, Supporting Information) and

maintained perfect connections between fibers. Note that the LM's role is indispensable as the conductivity of CuC is very sensitive to strain (**Figure S2b**, Supporting Information).

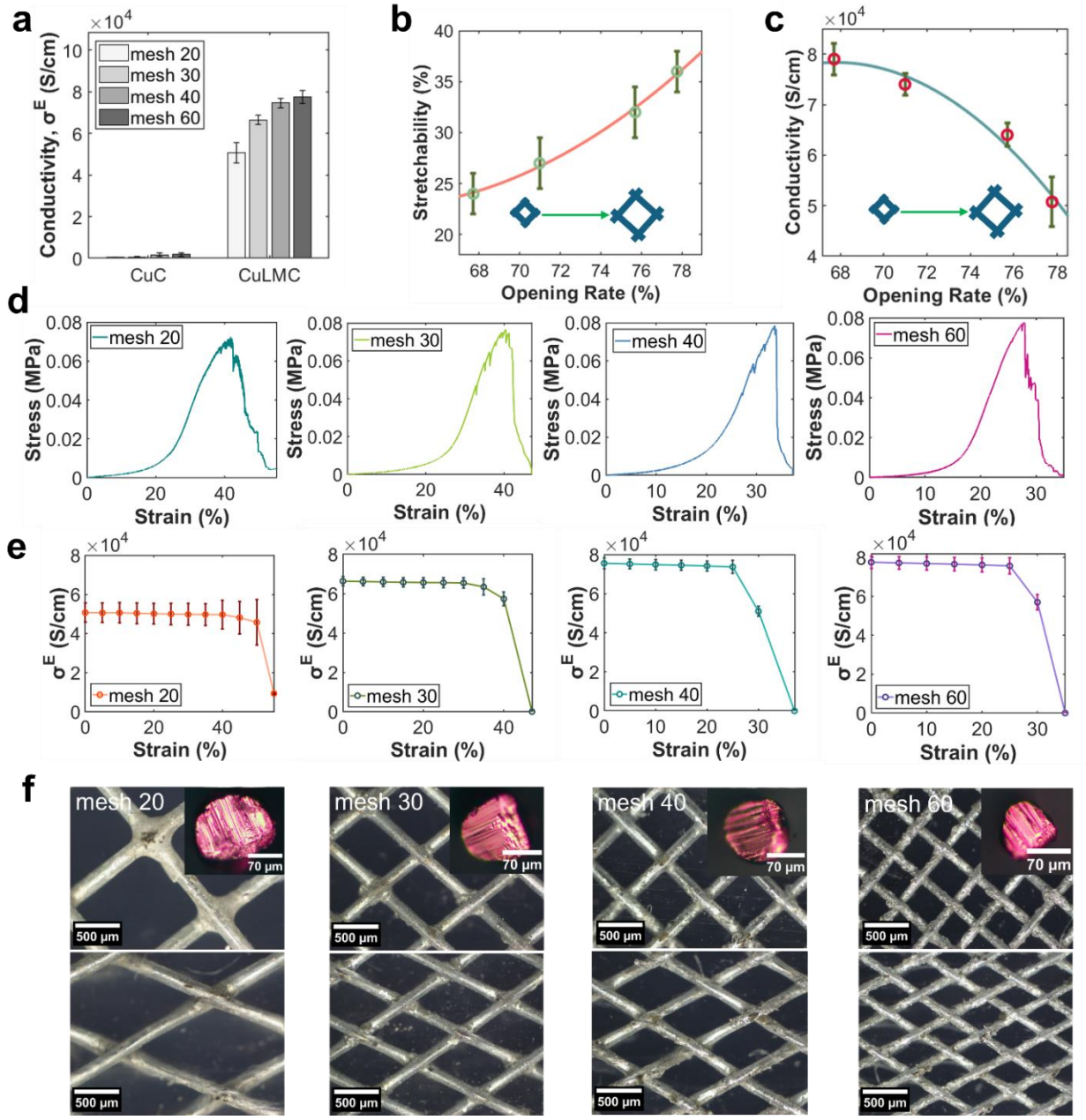

Figure 3. Electromechanical performance of CuCs and CuLMCs. a) CuLMCs demonstrate 20- to 60-fold conductivity increase compared to CuCs, owning to the LM junctions. b) Relationship between stretchability and opening rate of CuLMCs. c) Relationship between conductivity and opening rate. d) Mechanical behavior of CuLMCs with different mesh sizes. e) Electrical conductivity of CuLMCs under stretch for different mesh sizes. f) Optical microscopy images of CuLMCs. Typical cross-sectional profiles of individual fibers are on the top right corners. Both the original state (top row) and stretched state (bottom row, 32% strain for mesh #20, 25% for mesh #30, 24% for mesh #40, and 20% for mesh #60) are presented.

3.3. Enhance Stretchability using Angled Mesh. The stretchability of the CuLMCs can be improved by using angled mesh, i.e., applying prestrain to adjust the intersectional angle of the mesh before encapsulation. The mechanism is easy to understand (**Figure S1** and **Figure S3**, Supporting Information). Due to the geometric feature of the copper mesh, a pre-compressed mesh (**Figure 4a**) exhibits increased stretchability compared to the original one, with some sacrifice of the electrical conductivity due to the dimension change. For example, we are able to increase the maximum strain of a mesh #40 CuLMC from 25% to 100% by applying a -33% prestrain to the mesh before encapsulation. Hence, by employing prestrain, we can obtain composites with unprecedented conductivity and stretchability simultaneously, which is highly desirable for soft electronics applications. The relations between prestrain, conductivity, and stretchability of the CuLMCs with prestrain can be derived analytically from the geometric relations (**Equations S3** to **S6**, Supporting Information). **Figures 4b** and **4c** present the influence of prestrain on the conductivity and stretchability for CuLMCs with mesh #40. The theoretical solution agrees very well with experimental data. Generally, the stretchability enhancement will sacrifice conductivity to some extent. For example, a -33% prestrain would increase the stretchability by 4-fold (**Figure 4c**) but reduce the conductivity by a half (**Figure 4b**). Such general trends apply for other mesh sizes as well (**Figures S3** and **S6**, Supporting Information). In some cases, we are able to achieve above 150% stretchability for mesh #20 (**Figures S4** and **S8**, Supporting Information). In short, CuLMCs can be precisely tailored through prestrain to meet desired levels of conductivity and stretchability for soft electronic devices, and the theoretical formulae (**Equation S4** and **S6**, Supporting Information) can provide guidance for such design.

To examine the electromechanical performance of the CuLMCs with prestrain, four different types of composite samples with prestrain 0% (i.e., no prestrain), -10%, -20%, and -33% were fabricated using mesh #40 and tested under uniaxial loading. Electromechanical tests (**Figure 4d**, **4e**) suggest that prestrained CuLMCs have similar hyperelastic responses and strain-insensitive conductivity compared to the original one in **Figure 3**. For example, -20% prestrain would result in a conductivity of 58,000 S/cm, close to 10% of pure copper, with a stretchability of 55%. Similar performance was also found for other CuLMCs as listed in **Table S2**, Supporting Information. Such excellent properties are well suited for applications as flexible interconnects.

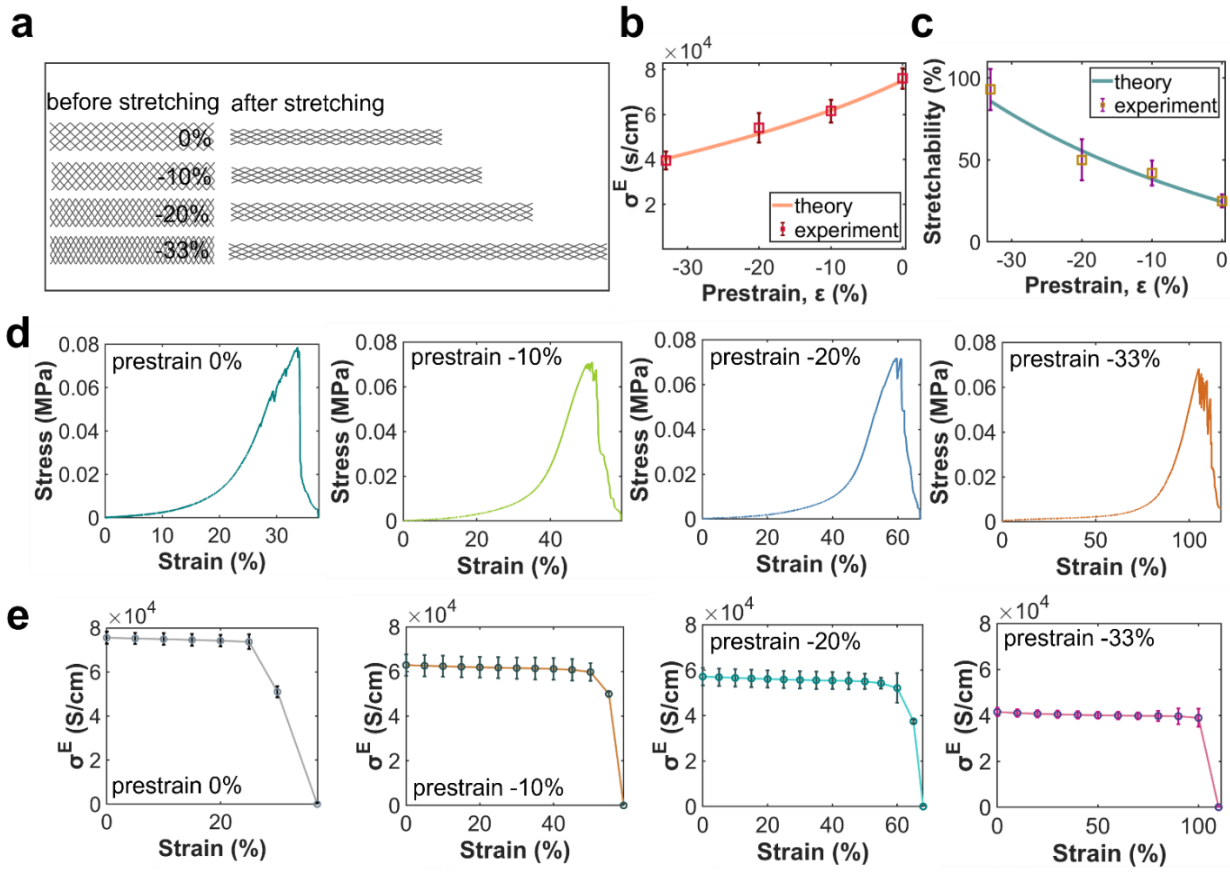

Figure 4. Electromechanical performance of CuLMCs embedded with angled (or prestrained) copper mesh to enhance their stretchability. All data are for mesh size #40 only. The stretchability of the composite can

be improved significantly by applying prestrain to the mesh, albeit sacrificing the conductivity to some extent. a) The pre-compressed mesh has increased stretchability compared to the original one due to the microstructural change. The stretchability of the composite increases from 20% to 100% by applying -33% of prestrain to the mesh. b) Electrical conductivity of CuLMCs under different prestrain level. c) Stretchability of CuLMCs under different prestrain level. d) Stress-strain behaviors of CuLMCs with 0%, -10%, -20%, and -33% prestrain. e) Conductivity-strain behaviors of CuLMCs with different prestrain. The conductivity is overall strain-insensitive until failure occurs.

3.4. Bending Performance. The CuLMCs have remarkable electrical performance under bending deformation, which is also a prominent indicator of flexible electronics. As the CuLMC film is very thin, a supporting polymer layer (polylactic acid sheet, thickness 110μm) is used to obtain uniform tensile bending mode.[48] As shown in **Figure 5a**, this bi-layer design has a substrate radius *r* in a range of 3.4-41 mm. As each mesh size has a different film thickness, the relation between the bending strain and substrate radius is shown in **Figure 5b**. It is observed that for the same substrate radius, a thicker film (e.g., mesh #20) produces greater bending strain compared to the thinner one (e.g., 60 mesh). The bending performance of CuLMCs is characterized by the normalized resistance R/R_0 (herein R_0 and R are resistance before and after bending) versus the bending strain. As shown in **Figure 5c-f**, the normalized resistance R/R_0 remains stable in a wide range of bending strain and only varied by a marginal factor of 2-4%. Even at 4% bending strain (i.e., r = 4-5 mm), these composites show promisingly strain-insensitive resistance, which is around 1.44-1.50mΩ/sq. The normalized resistance of mesh #20 CuLMC (**Figure 5c**) has a slightly larger variance compared to others due to its low opening rate and larger thickness. Considering the flexible electronics applications, conductive composites should have a bending radius of 1-5 mm[49] with an electrical performance degradation of less than 10%.[50] The bending test results of the CuLMCs show stable electrical responses (with 2-4% variation) even at a bending radius of 4-

5 mm. Therefore, CuLMC has the potential in the application of flexible electronics like wearable interconnectors and flexible devices with stable conductivity.

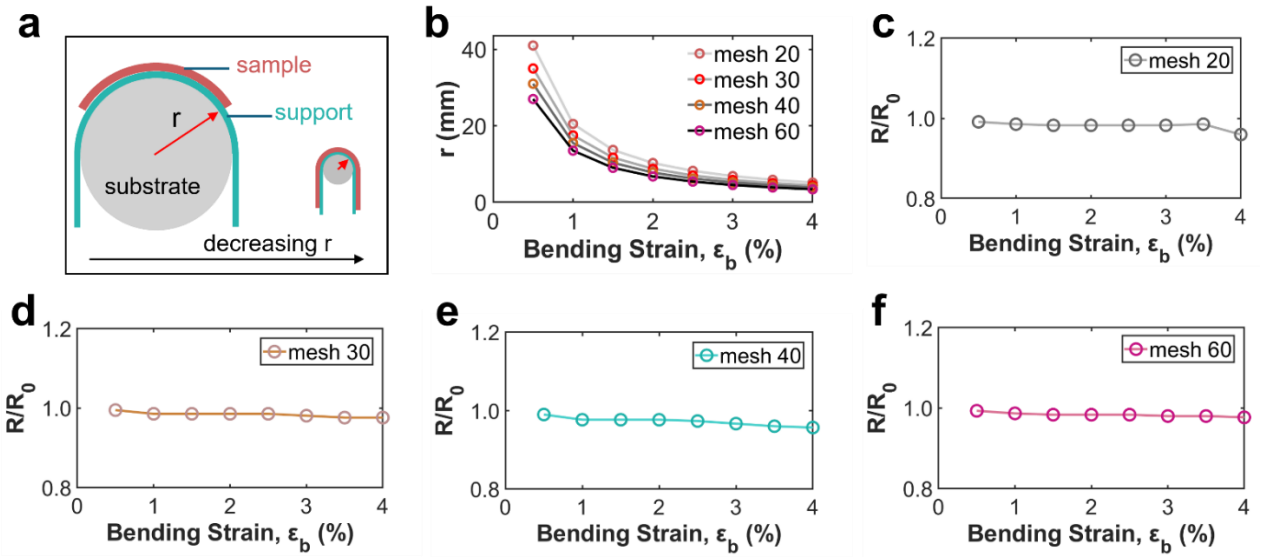

Figure 5. Electromechanical behavior of CuLMCs under bending deformation. a) Illustration of the test setup and bending radius of the substrate. CuLMC is mounted on a flexible support and then bent on a substrate with specific radius. b) The relationship between bending strain and substrate radius for each CuLMC. c-f) Normalized resistance versus bending strain of CuLMCs for different mesh sizes.

3.5. Cyclic Performance and Anti-aging Coating. The cyclic performance of CuLMCs is critical for their applications in soft electronics. We found that the corrosive reaction[51] between Cu and LM has a significant impact on the cyclic performance of CuLMCs, and discovered that a carbon coating on the copper mesh would resolve this problem.

As shown in **Figure 6**, we have recorded resistance changes when the composites experienced cyclic stretch (triangular strain profile, 0 to 15%) for 1000 cycles. Firstly, we examined the influence of Cu-LM reaction on the cyclic performance of CuLMCs (without carbon coating). We conducted cyclic testing for two samples on day 1 (**Figure 6a**) and day 14 (**Figure 6b**) after

fabrication to examine the aging effect. On day 1, optical microscopy images in **Figure 6a** show no sign of corrosive reaction and the junction region contains sufficient LM with a bright metallic color. The cyclic resistance response is also very stable on day 1. After 1000 cycles, normalized resistance R/R_0 changed in the range of 1.004 to 1.014, about 1% fluctuation. In contrast, the aging or corrosion process has a significant impact on the cyclic performance after 14 days. In **Figure 6b**, the optical microscopy images show that the fiber surface becomes dark and LM disappears at junctions, evidencing corrosive reactions between Cu and LM and the formation of intermetallic compound $CuGa_2$.[52] Meanwhile, the cyclic resistance response in **Figure 6b** is unstable given that the normalized resistance changes significantly after just 100 cycles.

To suppress the corrosion process, we deposited a thin carbon coating on the copper mesh before LM coating, as illustrated in **Figure 2**. Such a thin carbon coating serves as a barrier between Cu and LM to suppress corrosion [53] and preserve the LM junction. We choose carbon coating also because that it is highly conductive and would not impair the electrical conductivity of the composite. Certainly, other noble metal deposition may work as well if the wetting condition is good. **Figure 6c** shows the cyclic performance of a CuLMC sample (with carbon coating) after 14 days of fabrication. By comparing **Figure 6a** and **6c**, the composites with carbon coating showed a negligible aging effect after 14 days. The normalized resistance of the composite in **Figure 6c** is very stable and fluctuates within a 1% range. Besides the stable cyclic resistance performance, optical microscopy images in **Figure 6c** confirm that the corrosive reaction between Cu and LM is unnoticeable and sufficient LM exists in the junctions and surfaces after 14 days. Hence, we conclude that a barrier coating such as a thin carbon layer on the copper mesh is necessary to guarantee the cyclic performance of CuLMCs.

We also tested the stress-strain responses of the CuLMCs under cyclic loading. The CuLMCs exhibit some extent of viscoelastic behaviors, given that there is a hysteresis effect during cyclic loading (**Figure S10a**, Supporting Information). Such a viscoelastic behavior potentially arises from the fiber-fiber friction and intrinsic viscoelastic nature of the Ecoflex 00-30 matrix.[54] Oxidation of the LM phase may contribute to the viscoelastic behaviors as well but the influence may be marginal. In contrast to the viscoelastic behavior, no hysteresis was observed for the cyclic conductivity-strain responses (see **Figure S10b**, Supporting Information).

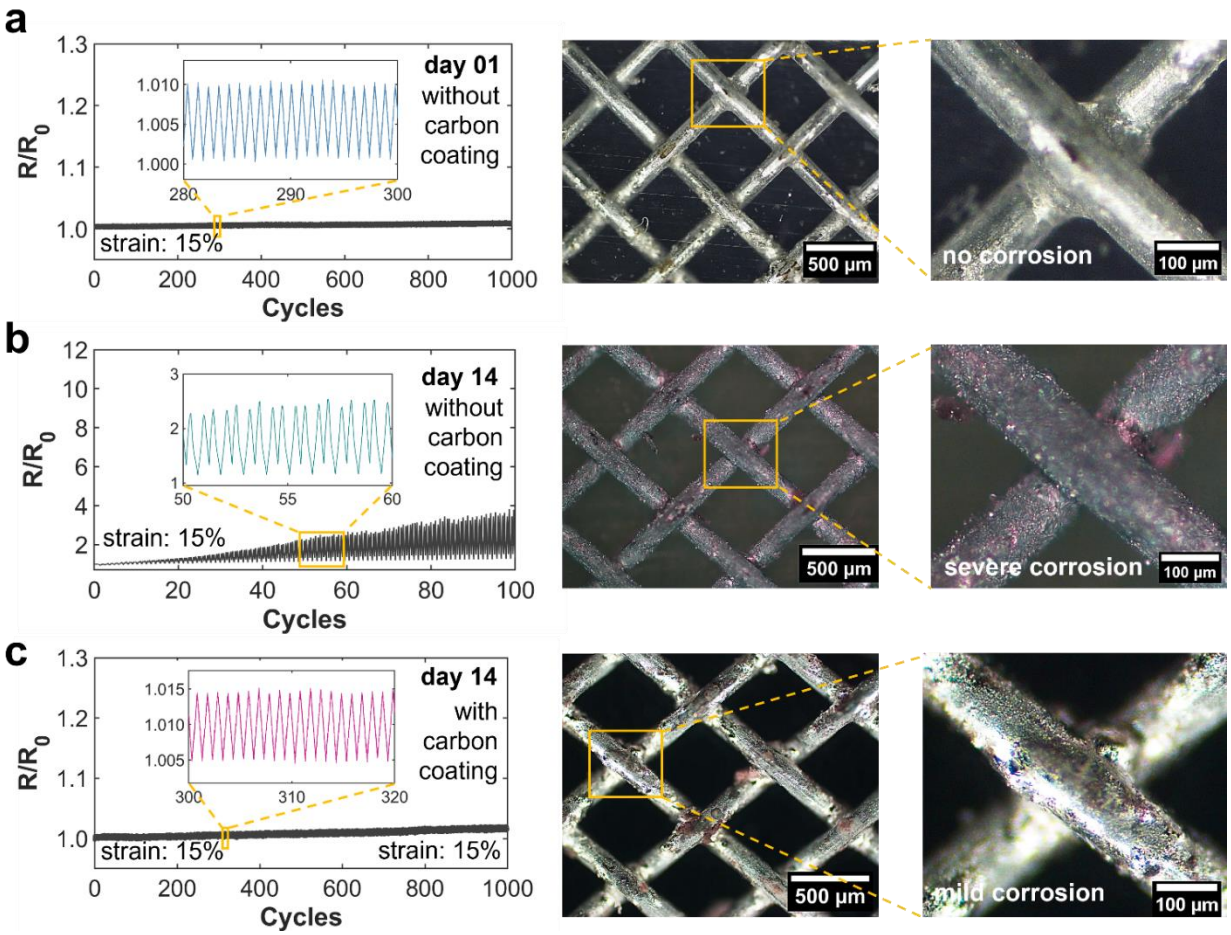

Figure 6. Cyclic electromechanical behavior of mesh #40 CuLMCs. a) Even without carbon coating, the as-fabricated composite has good cyclic performance with stable normalized resistance R/R_o. The OM images indicate the presence of sufficient LM in the junction. b) After 14 days of aging, the composite without carbon coating shows deteriorated performance under cyclic stretch. Optical microscopy images

indicate that the Cu surface becomes darker and the LM junction disappears. This is due to the corrosive reaction between LM and Cu. Consequently, the cyclic testing data shows a large deviation of R/R_o. c) Adding carbon coating on the copper mesh significantly suppresses the aging process and enhances the cyclic stability of the composite. The optical microscopy images show the presence of LM on the surface and junctions after 14 days. The aging process can be suppressed further by depositing thicker carbon coatings.

3.6. Strain-Insensitive Joule Heating Behavior. The strain-insensitive conductivity behavior of the proposed mesh composite with LM junctions is ideal to be employed as highly stretchable and strain-insensitive Joule heaters. For this application, we replace the Cu mesh with a brass mesh as the latter is more suited for Joule heating purposes for its higher Joule heating rate. The Joule heating behaviors of the brass mesh composites are presented in **Figure 7**. In **Figure 7a-b**, we compare the Joule heating performance of brass mesh composites before and after adding LM junctions, which are shown in **Figure 7a** and **7b**, respectively. The thermal images in **Figure 7a-b** indicate that LM junctions remarkably improve the heating uniformity. **Figure 7a-b** also show that brass mesh composite with LM junctions reach higher and more consistent surface temperatures, owning to reduced contact resistance between fibers. The Joule heating performance and power consumption are compared and presented in **Figure S15**, Supporting Information.

Figure **7c-d** show the influence of mechanical strain (0%, 15%, and 30%) and LM junctions on the temperature evolution of the brass mesh composites at fixed voltages (1.0V or 0.8V). Herein, **Figure 7c** and **7d** show results of the samples without and with LM junctions, respectively. From **Figure 7d**, we observe that LM junctions enable the composite Joule heaters with strain-insensitive Joule heating behavior under stretching, which cannot be achieved without the LM junctions (**Figure 7c**). Furthermore, **Figure 7e** shows the strain-insensitive Joule heating behavior of the brass-LM composites with LM junctions under various deformation modes such as

stretching, bending, and twisting without influencing average surface temperatures. The Ashby chart (**Figure 7f**) compares normalized surface temperature ($\Delta T/T_0$) with present literature and evidently shows that the proposed brass-LM composites have the highest stretchability (140% strain) with strain-insensitive Joule heating performance. The angled mesh brass-LM heater shows very high stretchability (**Figure S13**, Supporting Information) with uniform heat distribution and marginal temperature drift under stretching. In addition, the heater exhibited excellent environmental stability, maintaining consistent performance over 20 days **(Figure S14**, Supporting Information). Furthermore, it demonstrated robust cyclic heating reliability with negligible degradation observed across repeated thermal actuation cycles (**Figure S14e**, Supporting Information).

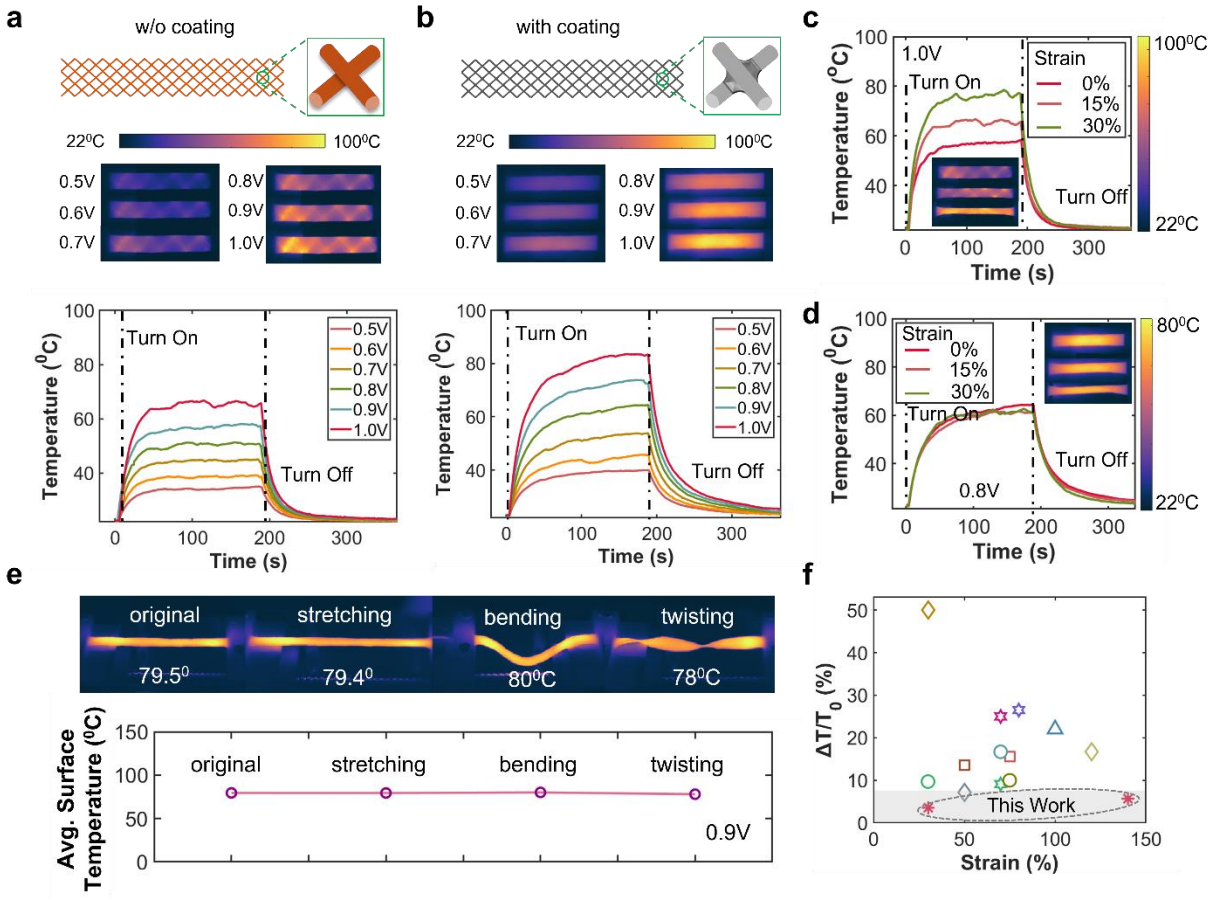

Figure 7. Strain-insensitive joule heating performance of brass mesh composites with LM junctions. a) Brass #30 mesh composites without LM junctions exhibit poor inter-fiber conductivity, localized heating, and thermal inconsistency. b) Brass #30 mesh composites with LM junctions (brass-LM composites) exhibit improved conductivity with more uniform and efficient heating performance. c) Temperature evolution profile of brass mesh composite without LM junctions under stretching. d) Temperature evolution profile of brass mesh composite with LM junctions under stretching. e) Average surface temperature of brass mesh composite with LM junctions under various deformation modes. Strain-insensitive Joule heating performance is observed. f) The Ashby chart shows that the strain-insensitive Joule heating behavior of the proposed brass-LM composites outperforms others with low thermal drift under large strain. Detailed data are tabulated in **Table S7**, Supporting Information.

3.7. Stretchable and Wearable Circuits. To empirically validate the performance, we have implemented CuLMC in a stretchable circuit (**Figure 8a**). In this setup, narrow strips of CuLMC

are connected to LEDs, designed to withstand a variety of mechanical deformation modes. When a voltage is applied, the assembly endures 50% stretching, about 90^0 twisting, and significant twisting/bending. Remarkably, throughout this rigorous process, the LEDs maintain their initial luminosity consistently. The resilience under mechanical stress, combined with electrical performance, potentially unleashes the application in wearable electronics and soft robotics as well. To investigate the compatibility with wearable electronics, CuLMC was integrated with multiple flat LEDs. As an attempt for complex shapes, integrated LEDs with CuLMC strips are connected as a BU-shaped structure. Later, the whole system is transferred and attached to a textile clothing surface. Normally, textile clothing withstands multi-directional deformation. To mimic real-world wearability, various deformation is also applied (**Figure 8b**). The vertical and diagonal elongation on clothing shows that the illumination of LEDs remains stable, which is a potential indication of better circuit functionality and integrity. Exceptional conditions mimicry (**Figure S11**, Supporting Information) such as simultaneous multi-directional bending, rolling, and bending-stretching also exhibited plausibly strain-insensitive conductivity. In the realm of wearable electronics, strain insensitivity is highly suitable for dynamic display and health monitoring devices, where maintaining functionality under stress conditions is decisive.

3.8. Capacitive Pressure Sensor. Pressure or tactile sensors are useful elements for wearable and flexible electronics, soft electronics, virtual reality, etc. As CuLMCs are strain-insensitive, highly conductive, flexible, and stretchable, they would be a good candidate for the capacitive pressure sensor. We have fabricated a capacitive pressure sensor as a sandwich structure by embedding a polyurethane foam layer in the middle and CuLMCs as top-bottom electrodes. The middle layer functions as a diaphragm keeping a certain distance between the electrodes. The actuation mode works based on the parallel distance and surface area of CuLMC electrodes. As

shown in **Figure 8c**, when pressure is applied, the thickness of the middle layer decreases and induces a higher capacitance value. To measure the effectiveness of the actuation principle, various modes of tactile feedback are tested, for instance, normal touch (**Figure 8d**), and haptic touch (**Figure 8f**). For normal touch, it changes the distance and hence the capacitance value, which is reflected by the relative change of capacitance ($\Delta C/C_0$). To check the maximum sensitivity range (**Figure 8e**), the sensor undergoes maximum compression, where it shows approximately 2.5 times shift in sensitivity than the initial value, which means the sensor has a very high sensitivity range. As CuLMCs are flexible, the sensor is capable of detecting haptic touch (**Figure 8f**) such as soft, medium, and hard, which would be potentially useful for designing adaptive robotic hands and smart grippers. To check the viability, another interesting prospect is demonstrated by grabbing a coffee cup (**Figure 8g**). In this case, the sensor was mounted on the palm of the right hand, and in situ capacitance data was then recorded before and after grabbing the object. As the hand palm folded, the sensor triggered the capacitance response and resulted in an abrupt rise in the graph.

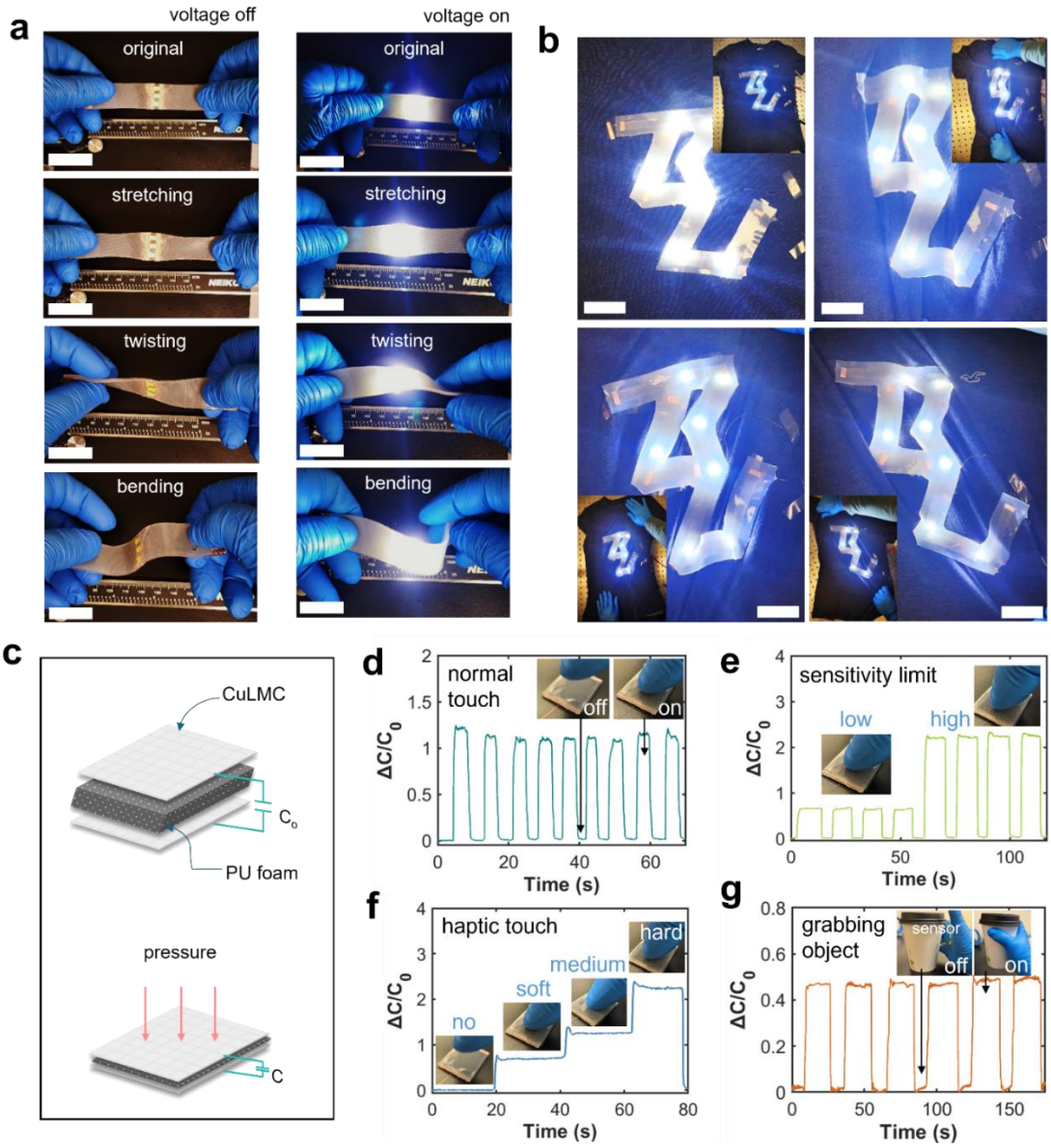

Figure 8. Application of CuLMCs as circuits, wearable interconnects, and pressure/tactile sensors. a) The stretchable circuit is incorporated with surface-mount LEDs backed by CuLMC. CuLMC can endure mechanical deformation in various modes such as stretching, bending, and twisting without compromising the brightness of LEDs. Scale bar 3cm. b) BU-shaped wearable interconnects attached to a textile garment. The interconnect is stretched in vertical and diagonal directions. Scale bar 3cm. c) Schematic of capacitive pressure sensor fabricated as a sandwich structure. d) Normal touch response on the sensor leads to variations in relative capacitance ($\Delta C/C_o$). e) Sensitivity limit measurement by compression. f) Capacitance responses in different levels of touch (haptic mode). g) Pressure response before and after grabbing an object. The sensor is attached to the hand palm.

3.9. Stretchable Heater, Heat Activated Transparency and Thermo Responsive Bending. Reliable thermal uniformity and strain-insensitive Joule heating performance are desired for flexible and wearable Joule heaters. **Figure 9** illustrates the Joule heating performance of flexible heaters and actuators. A strip of brass-LM composite heater is attached to a human knee (**Figure 9a**) to demonstrate thermotherapy application. It demonstrates mechanical robustness with stable temperature output (50.3°C straight and 49.6°C stretched). The soft Joule heater can also be wrapped around cylindrical and curved surfaces like a vial or pipe. In addition, such a soft Joule heater can also be used for thermal actuation as presented in **Figure 9b-c**. Herein, a switchable transparency actuator is fabricated with a brass-LM composite film as the heating source. PDMS and PW are used to encapsulate the brass-LM film. The actuator is opaque at room temperature but quickly turns transparent when voltage heats it above PW's melting point, revealing the text behind it. Thermo-responsive bending actuation (**Figure 9c**) is achieved using a thin solidified PW layer (300μm). It keeps the actuator flat initially when the voltage is off and bends progressively as the voltage heats PW from solid to liquid phase.

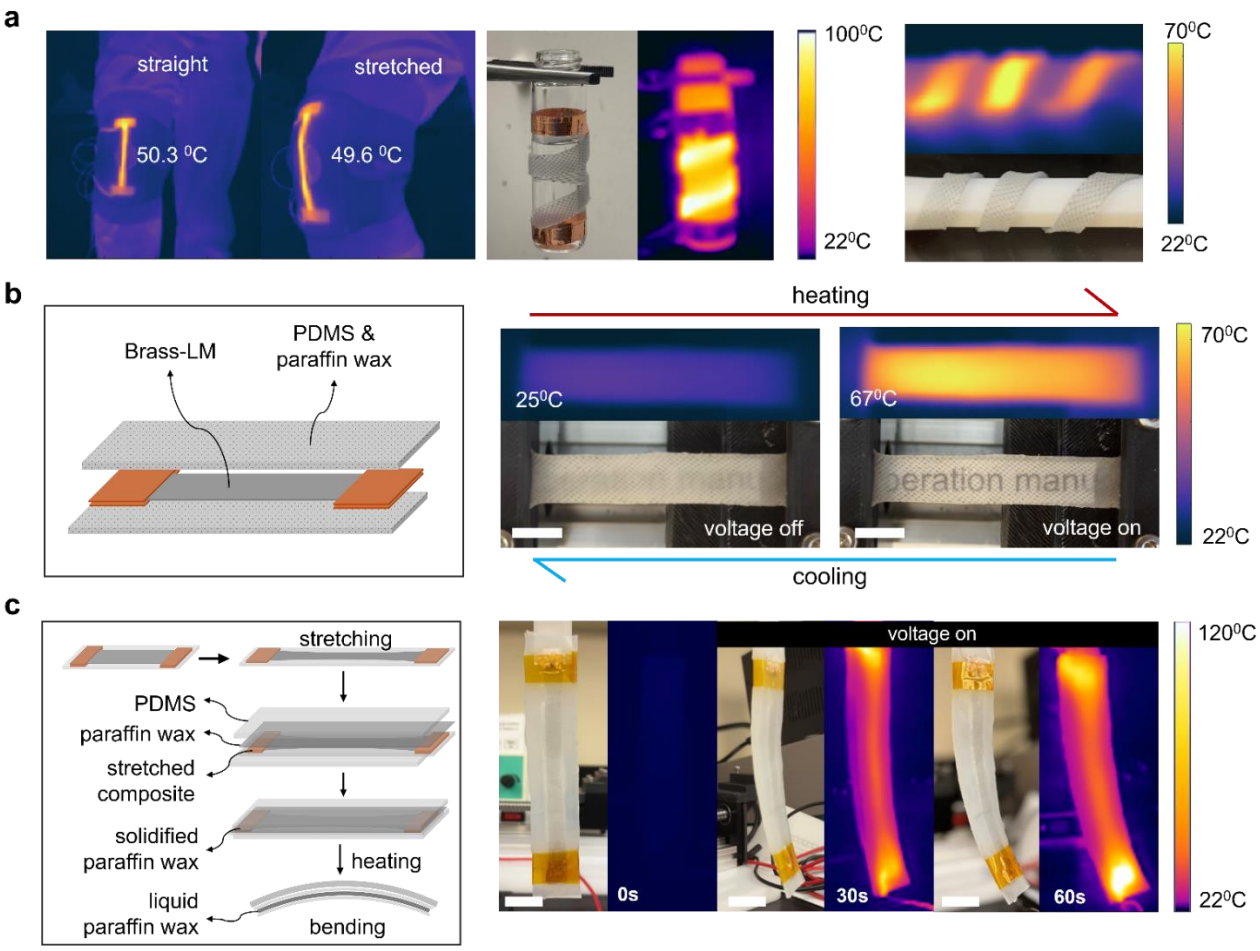

Figure 9. Applications of the brass-LM composites as highly stretchable and strain-insensitive Joule heaters. a) Surface adaptability of flexible heaters for thermotherapy (left) and wrapping heaters (middle and right). b) Schematic and performance of a heat-activated switchable transparency actuator. c) Schematic and demonstration of heat-based bending actuation.

4. CONCLUSION

In this work, we propose a new design concept for soft conductive composites to achieve high conductivity and stretchability simultaneously. It is well known that soft conductors usually suffer from a conductivity-stretchability tradeoff as these two properties usually oppose each other. By examining existing soft conductive composites, we conclude that soft composites with hybrid solid-liquid fillers are the most promising approach to overcome this tradeoff and attain high

performance. In order to achieve both high conductivity and stretchability, the hybrid composites need to have a primary solid network offering conductivity and a secondary liquid network offering stretchability. Employing this concept, we proposed a new class of soft conductive composites named CuLMCs, which consist of a woven copper fiber network, LM-based soft junctions, and a compliant elastomer matrix. The copper fiber network serves as the primary network, highly conductive and stretchable. Meanwhile, the LM junctions mitigate the contact resistance at fiber junctions without influencing their mobility and stretchability. Both the microstructural design and contract resistance treatment are needed to achieve high performance. This 'soft conductive junction' concept shows advantages over the contemporary hard junction approach in terms of conductivity and stretchability.

Our experimental results indicate that these CuLMCs exhibit several prominent features such as high conductivity (up to 77,000 S/cm), high stretchability (up to 180%), strain-insensitivity, and cyclic stability. For flexible electronics applications, the current target performance of development is 40,000-60,000 S/cm conductivity (10% of copper) under 30% stretch. Some of our CuLMCs can achieve conductivity around 60,000 S/cm under 45-70% stretch, which are remarkable values for soft conductors. In addition, using a similar design, we also achieve strain-insensitive Joule heating behavior for strain up to 140%. In brief, CuLMCs have pushed the current limit of soft conductors in terms of conductivity and stretchability. Notably, we also discovered that adding a carbon coating on the copper network will suppress corrosion and increase the lifespan of the materials. Overall, the ultra-high and strain-insensitive conductivity, high stretchability, and cyclic stability have enabled CuLMCs promising applications in soft and flexible electronics, soft sensors, soft robotics, stretchable Joule heaters, etc. Some potential applications have been demonstrated in this work.

Future research is much needed for the manufacturing of these hybrid woven network composites with finer feature sizes to broaden their applications in stretchable electronics. In addition, it would also be very interesting to discover other microstructural designs for the woven networks towards better performance.

ASSOCIATED CONTENT

Supporting Information

The Supporting Information is available free of charge on the ACS Publications website.

AUTHOR INFORMATION

Corresponding Author

Pu Zhang. Email: pzhang@binghamton.edu

Author Contributions

P.Z. supervised the project and revised the manuscript. A.R. and P.Z. introduced the concept. A.R. and J.M. designed the experimental methods. A.R. performed all experiments. M.M. performed simulations. A.R. wrote the first draft. All authors contributed to the review of the manuscript.

Notes

The authors declare no competing financial interest.

ACKNOWLEDGMENTS

This work was supported by the National Science Foundation through the award CMMI-2143297. The authors also thank the support from the Small Scale Systems Integration and

Packaging (S3IP) Center of Excellence, funded by the New York Empire State Development's Division of Science, Technology, and Innovation.

REFERENCES

(1) Kaltenbrunner, M.; Sekitani, T.; Reeder, J.; Yokota, T.; Kuribara, K.; Tokuhara, T.; Drack, M.; Schwödiauer, R.; Graz, I.; Bauer-Gogonea, S.; Bauer, S.; Someya, T. An Ultra-Lightweight Design for Imperceptible Plastic Electronics. *Nature* **2013**, *499* (7459), 458–463. https://doi.org/10.1038/nature12314.

(2) Dickey, M. D. Stretchable and Soft Electronics Using Liquid Metals. *Adv. Mater.* **2017**, *29* (27), 1606425. https://doi.org/10.1002/adma.201606425.

(3) Won, D.; Bang, J.; Choi, S. H.; Pyun, K. R.; Jeong, S.; Lee, Y.; Ko, S. H. Transparent Electronics for Wearable Electronics Application. *Chem. Rev.* **2023**, *123* (16), 9982–10078. https://doi.org/10.1021/acs.chemrev.3c00139.

(4) Zhao, Z.; Xia, K.; Hou, Y.; Zhang, Q.; Ye, Z.; Lu, J. Designing Flexible, Smart and Self-Sustainable Supercapacitors for Portable/Wearable Electronics: From Conductive Polymers. *Chem. Soc. Rev.* **2021**, *50* (22), 12702–12743. https://doi.org/10.1039/D1CS00800E.

(5) Zhang, L.; Wang, Y.; Gui, J.; Wang, X.; Li, R.; Liu, W.; Sun, C.; Zhao, X.; Guo, S. Efficient Welding of Silver Nanowires Embedded in a Poly(Vinylidene Fluoride) Film for Robust Wearable Electronics. *Adv. Mater. Technol.* **2019**, *4* (2), 1800438. https://doi.org/10.1002/admt.201800438.

(6) Cheong, H.-G.; Triambulo, Ross. E.; Lee, G.-H.; Yi, I.-S.; Park, J.-W. Silver Nanowire Network Transparent Electrodes with Highly Enhanced Flexibility by Welding for Application in Flexible Organic Light-Emitting Diodes. *ACS Appl. Mater. Interfaces* **2014**, *6* (10), 7846–7855. https://doi.org/10.1021/am5011354.

(7) Celle, C.; Mayousse, C.; Moreau, E.; Basti, H.; Carella, A.; Simonato, J.-P. Highly Flexible Transparent Film Heaters Based on Random Networks of Silver Nanowires. *Nano Res.* **2012**, *5* (6), 427–433. https://doi.org/10.1007/s12274-012-0225-2.

(8) Sorel, S.; Bellet, D.; Coleman, J. N. Relationship between Material Properties and Transparent Heater Performance for Both Bulk-like and Percolative Nanostructured Networks. *ACS Nano* **2014**, *8* (5), 4805–4814. https://doi.org/10.1021/nn500692d.

(9) Ji, S.; He, W.; Wang, K.; Ran, Y.; Ye, C. Thermal Response of Transparent Silver Nanowire/PEDOT:PSS Film Heaters. *Small* **2014**, *10* (23), 4951–4960. https://doi.org/10.1002/smll.201401690.

(10) Kang, H.; Song, S.-J.; Sul, Y. E.; An, B.-S.; Yin, Z.; Choi, Y.; Pu, L.; Yang, C.-W.; Kim, Y. S.; Cho, S. M.; Kim, J.-G.; Cho, J. H. Epitaxial-Growth-Induced Junction Welding of Silver Nanowire Network Electrodes. *ACS Nano* **2018**, *12* (5), 4894–4902. https://doi.org/10.1021/acsnano.8b01900.

(11) Zhao, Y.; Kim, A.; Wan, G.; Tee, B. C. K. Design and Applications of Stretchable and Self-Healable Conductors for Soft Electronics. *Nano Converg.* **2019**, *6* (1), 25. https://doi.org/10.1186/s40580-019-0195-0.

(12) Yun, G.; Tang, S.-Y.; Lu, H.; Zhang, S.; Dickey, M. D.; Li, W. Hybrid-Filler Stretchable Conductive Composites: From Fabrication to Application. *Small Sci.* **2021**, *1* (6), 2000080. https://doi.org/10.1002/smsc.202000080.

(13) Ma, J.; Liu, Z.; Nguyen, Q.-K.; Zhang, P. Lightweight Soft Conductive Composites Embedded with Liquid Metal Fiber Networks. *Adv. Funct. Mater. n/a* (n/a), 2308128. https://doi.org/10.1002/adfm.202308128.

(14) Won, P.; Kim, K. K.; Kim, H.; Park, J. J.; Ha, I.; Shin, J.; Jung, J.; Cho, H.; Kwon, J.; Lee, H.; Ko, S. H. Transparent Soft Actuators/Sensors and Camouflage Skins for Imperceptible Soft Robotics. *Adv. Mater.* **2021**, *33* (19), 2002397. https://doi.org/10.1002/adma.202002397.

(15) Yang, Y.; Wu, Y.; Li, C.; Yang, X.; Chen, W. Flexible Actuators for Soft Robotics. *Adv. Intell. Syst.* **2020**, *2* (1), 1900077. https://doi.org/10.1002/aisy.201900077.

(16) Wang, J.; Gao, D.; Lee, P. S. Recent Progress in Artificial Muscles for Interactive Soft Robotics. *Adv. Mater.* **2021**, *33* (19), 2003088. https://doi.org/10.1002/adma.202003088.

(17) Park, M.; Park, J.; Jeong, U. Design of Conductive Composite Elastomers for Stretchable Electronics. *Nano Today* **2014**, *9* (2), 244–260. https://doi.org/10.1016/j.nantod.2014.04.009.

(18) Zhang, Y.; Zhang, Y.; Zhou, J.; Zhang, D.; Lin, H.; Chen, Y.; Li, Y.; Xiong, J. Stretchable Composite Conductive Fibers for Wearables. *Adv. Mater. Technol.* **2023**, *8* (6), 2201442. https://doi.org/10.1002/admt.202201442.

(19) Choi, S.; Han, S. I.; Kim, D.; Hyeon, T.; Kim, D.-H. High-Performance Stretchable Conductive Nanocomposites: Materials, Processes, and Device Applications. *Chem. Soc. Rev.* **2019**, *48* (6), 1566–1595. https://doi.org/10.1039/C8CS00706C.

(20) Choi, S.; Han, S. I.; Jung, D.; Hwang, H. J.; Lim, C.; Bae, S.; Park, O. K.; Tschabrunn, C. M.; Lee, M.; Bae, S. Y.; Yu, J. W.; Ryu, J. H.; Lee, S.-W.; Park, K.; Kang, P. M.; Lee, W. B.; Nezafat, R.; Hyeon, T.; Kim, D.-H. Highly Conductive, Stretchable and Biocompatible Ag–Au Core–Sheath Nanowire Composite for Wearable and Implantable Bioelectronics. *Nat. Nanotechnol.* **2018**, *13* (11), 1048–1056. https://doi.org/10.1038/s41565-018-0226-8.

(21) Lee, W.; Kim, H.; Kang, I.; Park, H.; Jung, J.; Lee, H.; Park, H.; Park, J. S.; Yuk, J. M.; Ryu, S.; Jeong, J.-W.; Kang, J. Universal Assembly of Liquid Metal Particles in Polymers Enables Elastic Printed Circuit Board. *Science* **2022**, *378* (6620), 637–641. https://doi.org/10.1126/science.abo6631.

(22) Parida, K.; Thangavel, G.; Cai, G.; Zhou, X.; Park, S.; Xiong, J.; Lee, P. S. Extremely Stretchable and Self-Healing Conductor Based on Thermoplastic Elastomer for All-Three-Dimensional Printed Triboelectric Nanogenerator. *Nat. Commun.* **2019**, *10* (1), 2158. https://doi.org/10.1038/s41467-019-10061-y.

(23) Xu, F.; Zhu, Y. Highly Conductive and Stretchable Silver Nanowire Conductors. *Adv. Mater.* **2012**, *24* (37), 5117–5122. https://doi.org/10.1002/adma.201201886.

(24) Miyamoto, A.; Lee, S.; Cooray, N. F.; Lee, S.; Mori, M.; Matsuhisa, N.; Jin, H.; Yoda, L.; Yokota, T.; Itoh, A.; Sekino, M.; Kawasaki, H.; Ebihara, T.; Amagai, M.; Someya, T. Inflammation-Free, Gas-Permeable, Lightweight, Stretchable on-Skin Electronics with Nanomeshes. *Nat. Nanotechnol.* **2017**, *12* (9), 907–913. https://doi.org/10.1038/nnano.2017.125.

(25) Kayaharman, M.; Argasinski, H.; Atkinson, J.; Zhang, K.; Zhou, Y. N.; Goldthorpe, I. A. Enhancing and Understanding the High Stretchability of Printable, Conductive Silver Nanowire Ink. *J. Electron. Mater.* **2023**, *52* (7), 4634–4643. https://doi.org/10.1007/s11664-023-10417-7.

(26) Zrnic, D.; Swatik, D. S. On the Resistivity and Surface Tension of the Eutectic Alloy of Gallium and Indium. *J. Common Met.* **1969**, *18* (1), 67–68. https://doi.org/10.1016/0022-5088(69)90121-0.

(27) Ma, R.; Kang, B.; Cho, S.; Choi, M.; Baik, S. Extraordinarily High Conductivity of Stretchable Fibers of Polyurethane and Silver Nanoflowers. *ACS Nano* **2015**, *9* (11), 10876–10886. https://doi.org/10.1021/acsnano.5b03864.

(28) Cao, C.; Huang, X.; Lv, D.; Ai, L.; Chen, W.; Hou, C.; Yi, B.; Luo, J.; Yao, X. Ultrastretchable Conductive Liquid Metal Composites Enabled by Adaptive Interfacial Polarization. *Mater. Horiz.* **2021**, *8* (12), 3399–3408. https://doi.org/10.1039/D1MH00924A.

(29) Rogers, J. A.; Someya, T.; Huang, Y. Materials and Mechanics for Stretchable Electronics. *Science* **2010**, *327* (5973), 1603–1607. https://doi.org/10.1126/science.1182383.

(30) Wang, J.; Cai, G.; Li, S.; Gao, D.; Xiong, J.; Lee, P. S. Printable Superelastic Conductors with Extreme Stretchability and Robust Cycling Endurance Enabled by Liquid-Metal Particles. *Adv. Mater.* **2018**, *30* (16), 1706157. https://doi.org/10.1002/adma.201706157.

(31) Suh, Y. D.; Jung, J.; Lee, H.; Yeo, J.; Hong, S.; Lee, P.; Lee, D.; Ko, S. H. Nanowire Reinforced Nanoparticle Nanocomposite for Highly Flexible Transparent Electrodes: Borrowing Ideas from Macrocomposites in Steel-Wire Reinforced Concrete. *J. Mater. Chem. C* **2017**, *5* (4), 791–798. https://doi.org/10.1039/C6TC04529D.

(32) Yao, S.; Zhu, Y. Nanomaterial-Enabled Stretchable Conductors: Strategies, Materials and Devices. *Adv. Mater.* **2015**, *27* (9), 1480–1511. https://doi.org/10.1002/adma.201404446.

(33) Joo, H.; Jung, D.; Sunwoo, S.-H.; Koo, J. H.; Kim, D.-H. Material Design and Fabrication Strategies for Stretchable Metallic Nanocomposites. *Small* **2020**, *16* (11), 1906270. https://doi.org/10.1002/smll.201906270.

(34) Hajalilou, A.; Silva, A. F.; Lopes, P. A.; Parvini, E.; Majidi, C.; Tavakoli, M. Biphasic Liquid Metal Composites for Sinter-Free Printed Stretchable Electronics. *Adv. Mater. Interfaces* **2022**, *9* (5), 2101913. https://doi.org/10.1002/admi.202101913.

(35) Madadi, M.; Zhang, P. Finite-Size Effect on the Percolation and Electromechanical Behaviors of Liquid Metal Particulate Composites. *Soft Matter* **2024**, *20* (5), 1061–1069. https://doi.org/10.1039/D3SM01469J.

(36) Lim, J.-E.; Lee, S.-M.; Kim, S.-S.; Kim, T.-W.; Koo, H.-W.; Kim, H.-K. Brush-Paintable and Highly Stretchable Ag Nanowire and PEDOT:PSS Hybrid Electrodes. *Sci. Rep.* **2017**, *7* (1), 14685. https://doi.org/10.1038/s41598-017-14951-3.

(37) Feng, P.; Ye, Z.; Wang, Q.; Chen, Z.; Wang, G.; Liu, X.; Li, K.; Zhao, W. Stretchable and Conductive Composites Film with Efficient Electromagnetic Interference Shielding and Absorptivity. *J. Mater. Sci.* **2020**, *55* (20), 8576–8590. https://doi.org/10.1007/s10853-019-04172-6.

(38) Kang, H.; Yi, G.-R.; Kim, Y. J.; Cho, J. H. Junction Welding Techniques for Metal Nanowire Network Electrodes. *Macromol. Res.* **2018**, *26* (12), 1066–1073. https://doi.org/10.1007/s13233-018-6150-9.

(39) Wang, Y.; Zhang, L.; Wang, D. Ultrastretchable Hybrid Electrodes of Silver Nanowires and Multiwalled Carbon Nanotubes Realized by Capillary-Force-Induced Welding. *Adv. Mater. Technol.* **2019**, *4* (11), 1900721. https://doi.org/10.1002/admt.201900721.

(40) Woo, J. Y.; Kim, K. K.; Lee, J.; Kim, J. T.; Han, C.-S. Highly Conductive and Stretchable Ag Nanowire/Carbon Nanotube Hybrid Conductors. *Nanotechnology* **2014**, *25* (28), 285203. https://doi.org/10.1088/0957-4484/25/28/285203.

(41) Hauger, T. C.; Al-Rafia, S. M. I.; Buriak, J. M. Rolling Silver Nanowire Electrodes: Simultaneously Addressing Adhesion, Roughness, and Conductivity. *ACS Appl. Mater. Interfaces* **2013**, *5* (23), 12663–12671. https://doi.org/10.1021/am403986f.

(42) Park, J. H.; Hwang, G.-T.; Kim, S.; Seo, J.; Park, H.-J.; Yu, K.; Kim, T.-S.; Lee, K. J. Flash-Induced Self-Limited Plasmonic Welding of Silver Nanowire Network for Transparent Flexible Energy Harvester. *Adv. Mater.* **2017**, *29* (5), 1603473. https://doi.org/10.1002/adma.201603473.

(43) Yoon, S.-S.; Khang, D.-Y. Room-Temperature Chemical Welding and Sintering of Metallic Nanostructures by Capillary Condensation. *Nano Lett.* **2016**, *16* (6), 3550–3556. https://doi.org/10.1021/acs.nanolett.6b00621.

(44) Guo, R.; Wang, H.; Chen, G.; Yuan, B.; Zhang, Y.; Liu, J. Smart Semiliquid Metal Fibers with Designed Mechanical Properties for Room Temperature Stimulus Response and Liquid Welding. *Appl. Mater. Today* **2020**, *20*, 100738. https://doi.org/10.1016/j.apmt.2020.100738.

(45) Wang, S.; Liu, H.; Pan, Y.; Xie, F.; Zhang, Y.; Zhao, J.; Wen, S.; Gao, F. Performance Enhancement of Silver Nanowire-Based Transparent Electrodes by Ultraviolet Irradiation. *Nanomaterials* **2022**, *12* (17), 2956. https://doi.org/10.3390/nano12172956.

(46) Wang, S.; Tian, H.; Wang, Y.; Zuo, H.; Tao, C.; Liu, J.; Li, P.; Yang, Y.; Kou, X.; Wang, J.; Kang, W. Ruptured Liquid Metal Microcapsules Enabling Hybridized Silver Nanowire Networks towards High-Performance Deformable Transparent Conductors. *Nanoscale* **2024**, *16* (13), 6522–6530. https://doi.org/10.1039/D3NR06508A.

(47) Lide, D. R. *CRC Handbook of Chemistry and Physics, 85th Edition*; CRC Press, 2004.

(48) Kim, T.-W.; Lee, J.-S.; Kim, Y.-C.; Joo, Y.-C.; Kim, B.-J. Bending Strain and Bending Fatigue Lifetime of Flexible Metal Electrodes on Polymer Substrates. *Materials* **2019**, *12* (15), 2490. https://doi.org/10.3390/ma12152490.

(49) Kim, D.-H.; Lu, N.; Ma, R.; Kim, Y.-S.; Kim, R.-H.; Wang, S.; Wu, J.; Won, S. M.; Tao, H.; Islam, A.; Yu, K. J.; Kim, T.; Chowdhury, R.; Ying, M.; Xu, L.; Li, M.; Chung, H.-J.; Keum, H.; McCormick, M.; Liu, P.; Zhang, Y.-W.; Omenetto, F. G.; Huang, Y.; Coleman, T.; Rogers, J. A. Epidermal Electronics. *Science* **2011**, *333* (6044), 838–843. https://doi.org/10.1126/science.1206157.

(50) Lee, J.; Wu, J.; Ryu, J. H.; Liu, Z.; Meitl, M.; Zhang, Y.-W.; Huang, Y.; Rogers, J. A. Stretchable Semiconductor Technologies with High Areal Coverages and Strain-Limiting Behavior: Demonstration in High-Efficiency Dual-Junction GaInP/GaAs Photovoltaics. *Small* **2012**, *8* (12), 1851–1856. https://doi.org/10.1002/smll.201102437.

(51) Cui, Y.; Ding, Y.; Xu, S.; Yang, Z.; Zhang, P.; Rao, W.; Liu, J. Liquid Metal Corrosion Effects on Conventional Metallic Alloys Exposed to Eutectic Gallium–Indium Alloy Under Various Temperature States. *Int. J. Thermophys.* **2018**, *39* (10), 113. https://doi.org/10.1007/s10765-018-2440-x.

(52) Mu, G.; Qu, W.; Zhu, H.; Zhuang, H.; Zhang, Y. Low Temperature Cu/Ga Solid–Liquid Inter-Diffusion Bonding Used for Interfacial Heat Transfer in High-Power Devices. *Metals* **2020**, *10* (9), 1223. https://doi.org/10.3390/met10091223.

(53) Liu, G.; He, D.; Liu, J.; Xie, H.; Chen, Z.; Wei, C.; Xu, X.; Wang, P. Influencing Factors for Resistance Performance of Cu/C Composites to Liquid Ga Corrosion. *Mater. Today Commun.* **2023**, *35*, 105999. https://doi.org/10.1016/j.mtcomm.2023.105999.

(54) Liao, Z.; Hossain, M.; Yao, X.; Navaratne, R.; Chagnon, G. A Comprehensive Thermo-Viscoelastic Experimental Investigation of Ecoflex Polymer. *Polym. Test.* **2020**, *86*, 106478. https://doi.org/10.1016/j.polymertesting.2020.106478.